*Korean J. Chem. Eng.*, 35(3), 702-708 (2018)
DOI: 10.1007/s11814-017-0318-4

pISSN: 0256-1115
eISSN: 1975-7220

# Comparison of dye degradation potential of biosynthesized copper oxide, manganese dioxide, and silver nanoparticles using *Kalopanax pictus* plant extract

**Sun A. Moon, Bipinchandra K. Salunke, Pathikrit Saha, Aarti R. Deshmukh, and Beom Soo Kim†**

Department of Chemical Engineering, Chungbuk National University, Cheongju, Chungbuk 28644, Korea
(*Received 31 August 2017 • accepted 20 November 2017*)

**Abstract**−Copper(II) oxide (CuO), manganese dioxide ($MnO_2$), and silver (Ag) nanoparticles were synthesized using *Kalopanax pictus* plant extract. The nanoparticle synthesis was monitored using UV-visible spectra. The occurrence of each peak at 368, 404, and 438 nm wavelength indicated the synthesis of CuO, $MnO_2$, and Ag nanoparticles, respectively. The synthesized nanoparticles were characterized by X-ray photoelectron spectroscopy, energy dispersive X-ray spectroscopy, field emission scanning electron microscopy, and transmission electron microscopy. Catalytic potentials of the synthesized nanoparticles were compared to degrade two typical acidic and basic dyes (Congo red and Safranin O). The degradation ability of $MnO_2$ nanoparticles against Congo red was higher than that of Ag and CuO nanoparticles. All three types of nanoparticles showed a similar degradation ability against Safranin O over 80%. This study demonstrates that biologically synthesized nanoparticles using *Kalopanax pictus* are good agents for degradation of dyes.

Keywords: Biological Synthesis, Copper Oxide, Manganese Dioxide, Silver, Nanoparticles, Plant Extract, Dye Degradation

## INTRODUCTION

Nanoparticles, particles with a size up to 100 nm, exhibit unique physical and chemical properties compared with their bulk materials [1,2]. There is significant interest in obtaining well-dispersed, ultrafine and uniform nanoparticles to delineate and utilize their distinct properties [3]. Physical and chemical processes are common choices for the synthesis of nanoparticles. However, these methods involve the use of toxic chemicals in their synthesis protocols, which may create some hazardous effects in biomedical applications [4]. Therefore, development of nontoxic and ecofriendly methods for synthesis of nanoparticles is utmost important [5].

The biosynthesis of nanoparticles using microorganisms is one of the most important methods that employ bacteria, yeasts, or fungi in the process [6,7]. It has attracted attention of researchers due to its important role in remediation of toxic metals through reduction of the metal ions. However, the biological nanoparticle synthesis route generates nanoparticles at a much slower rate, a major drawback of biological synthesis. Biological synthesis would have greater commercial viability if the nanoparticles could be synthesized more rapidly and in large production scale [8,9]. Enzymes function as catalysts for the synthesis of metal nanoparticles [10]. Various enzymes, such as oxidase, hydroxylase, hydrolytic proteins, and $NAD(P)^+$-dependent enzymes, are applied to biocatalysts for the synthesis of metal nanoparticles [11]. Plants are good resources for bioactive chemicals [12]. Synthesis of nanoparticles using plant or plant extracts has an advantage over other biological synthesis of nanoparticles [3]. This method eliminates the step of cell culture and provides simple purification. It can also be suitably scaled up for large-scale synthesis of nanoparticles [13,14].

Metal and metal oxide nanoparticles are useful as catalysts and for various other applications due to their mildness, environmentally benign nature, convenience and use without additional templates and apparatus [15]. Copper(II) oxide (CuO) is a semiconducting compound with a narrow band gap. CuO nanoparticles gain great interest because of the natural abundance of their starting material, low cost production processing, nontoxic nature, and reasonably good electrical and optical properties, such as photoconductive and photothermal applications [16,17]. Recently, it has been emphasized that apart from the size, the shape of the nanostructure is equally important for controlling different properties such as optical absorption in CuO nanostructures and catalytic activity [18-20]. Manganese dioxide ($MnO_2$) nanoparticles have applications in medicine, catalysis, ion-exchange, molecular adsorption, biosensor and energy storage [15]. Silver (Ag) nanoparticles are receiving increasing attention because of their potential applications in medicine, forensic science, cosmetics, food chemistry, agriculture, and variety of other fields [14].

Dyes are usually used to color materials such as leather, plastics, textiles, food, paper, and cosmetics [21]. Estimates indicate that approximately 1-15% of the synthetic textile dyes used are lost in wastewater streams during manufacturing operations [22,23]. Presence of high concentration of dye in aquatic system has a tremendous effect on the health of humans, animals, and plants. Contamination of dye in water can cause allergic dermatitis, skin irritation, cancer, and mutation in human beings. Efforts have been already initiated to eliminate dye from water [24]. Many methods used for dye removal include chemical coagulation, flocculation, chemical oxidation, photochemical degradation, membrane filtration, and aerobic and anaerobic biological degradation [25,26]. Metal nanoparticles such as Ag nanoparticles are also employed

†To whom correspondence should be addressed.
E-mail: bskim@chungbuk.ac.kr
Copyright by The Korean Institute of Chemical Engineers.

for decolorization of the colored effluent. The use of Ag nanoparticles has shown rapid degradation ability with sustained reactivity compared to other decomposition techniques [26,27]. Ag nanoparticles synthesized using fruit extract of cucumber (*Cucumis sativus*) were examined by degradation of methylene blue under solar irradiation [28]. Nanocomposites of $MnO_2$ nanoparticles and fique fibers were successfully used to decompose indigo carmine with a maximum efficiency of 98.8% within 5 min [29].

In this study, in order to develop an eco-friendly and low cost process for the synthesis of nanoparticles, we synthesized CuO, $MnO_2$, and Ag nanoparticles using *Kalopanax pictus* plant extract as a reducing and stabilizing agent. *Kalopanax pictus* plant extract was chosen because it showed highest nanoparticle synthesis rate in the previous report [14]. The synthesized nanoparticles were characterized by UV-visible spectroscopy, X-ray photoelectron spectroscopy, energy dispersive X-ray spectroscopy, field emission scanning electron microscopy, and transmission electron microscopy. Catalytic potential of three types of biosynthesized nanoparticles (CuO, $MnO_2$, and Ag) was compared to degrade two typical acidic and basic dyes (Congo red and Safranin O) for the first time.

## MATERIALS AND METHODS

### 1. Reagents

The reagents used in this work include a plant (*Kalopanax pictus*), copper(II) sulfate pentahydrate ($CuSO_4 \cdot 5H_2O$; 99.0% purity, Duksan Chemical, Korea), potassium permanganate ($KMnO_4$; 99+% purity, Sigma-Aldrich, USA), silver nitrate ($AgNO_3$; 99.8% purity, Samchun, Korea), Congo red (dye content ~40%, Sigma-Aldrich, USA), Safranin O (dye content ≥85%, Sigma-Aldrich, USA).

### 2. Preparation of Plant Extract

Freshly collected green *Kalopanax pictus* plant leaves were washed and dried at room temperature for two days. The plant leaf extracts were prepared by taking 5 g of plant leaves in 100 ml of sterile distilled water and then boiling the mixture for 15 min before finally decanting it. The plant leaf extracts were stored at 4 °C and used within a week.

### 3. Biological Synthesis of Nanoparticles

A typical synthesis of CuO nanoparticles in solution phase was carried out as follows: $CuSO_4 \cdot 5H_2O$ was prepared as 1 mM aqueous solution and *Kalopanax pictus* plant leaf extract was added to 5% volume of the total solution. CuO nanoparticles were synthesized by stirring for 24 hours at 90 °C. Similarly, $MnO_2$ and Ag nanoparticles were synthesized using *Kalopanax pictus* plant leaf extract from 1 mM $KMnO_4$ by stirring for one hour at 30 °C and from 1 mM $AgNO_3$ by stirring for 2.5 hours at 30 °C, respectively [14,15]. The nanoparticle solution obtained was purified by repeated centrifugation at 15,000 rpm for 20 min followed by redispersion of the pellet in deionized water and then freeze dried.

### 4. Characterization of Nanoparticles

UV-visible spectra of the nanoparticles were taken with a UV-visible spectrophotometer. After freeze drying of the purified nanoparticles, the structure and composition were analyzed by transmission electron microscopy (TEM, Carl Zeiss, Libra 120), field emission scanning electron microscopy (SEM, LEO-1530), energy dispersive X-ray spectroscopy (EDS, LEO-1530), and X-ray photoelecron spectroscopy (XPS, Ulvax-PHI, PHI Quantera-II).

### 5. Dye Degradation

Dye degradation studies involved Congo red and Safranin O dyes. Dye solutions in water were prepared at a concentration of 20 ppm. The purified and freeze dried nanoparticles were added at a concentration of 10 g/L in dye solutions. The decolorization of dyes was monitored by UV-visible spectroscopy. Functional groups before and after reaction were analyzed by Fourier transform infrared spectroscopy (FT-IR, IR200, Thermo Scientific, Madison, WI, USA) in the wave number region of 4,000-400 $cm^{-1}$. Samples were prepared by placing a drop of the dye solution on the face of non-hygroscopic thallium bromoiodide disc (KRS-5, 25×4 mm, Thermo Scientific) and evaporating the water.

## RESULTS AND DISCUSSION

### 1. Characterization of Nanoparticles

The change in color of precursor solution after addition of *Kalopanax pictus* plant extract from colorless to yellow to brownish gave an indication of the synthesis of CuO nanoparticles (Fig. 1). The synthesis and characterization of CuO nanoparticles was

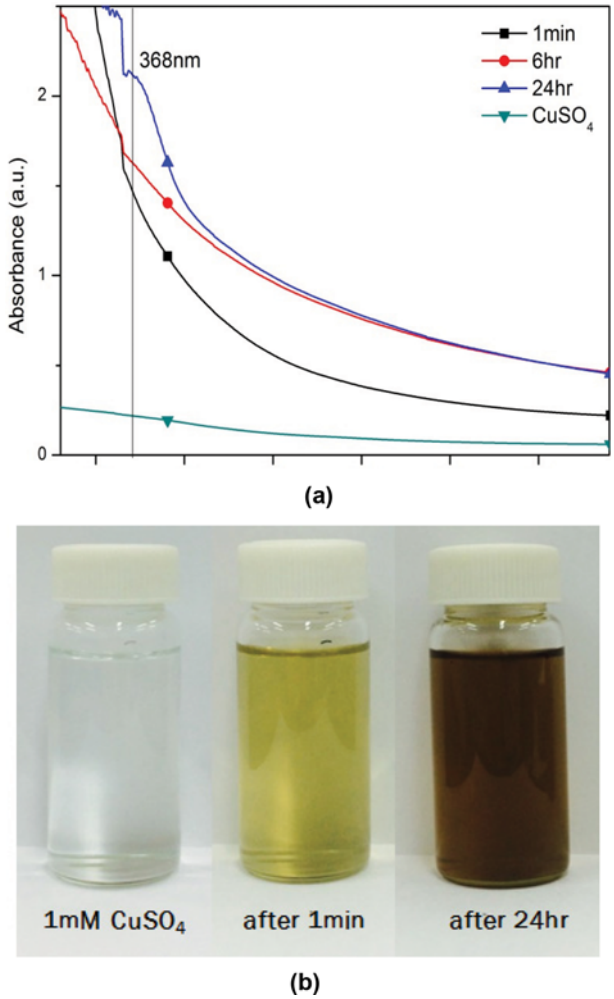


**Fig. 1. Time course of CuO nanoparticle synthesis by (a) UV-visible spectrophotometry and (b) color changes.**

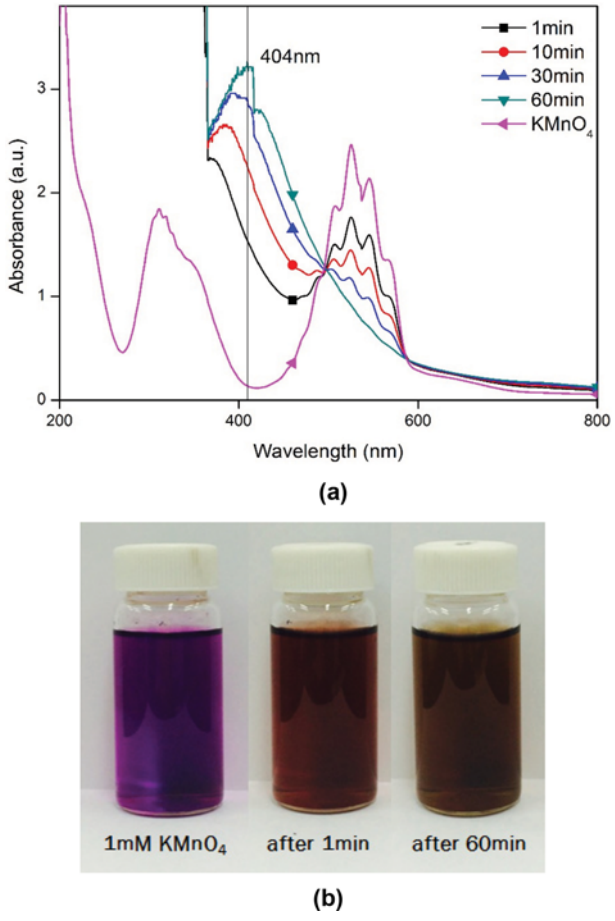


**Fig. 2. Time course of $MnO_2$ nanoparticle synthesis by (a) UV-visible spectrophotometry and (b) color changes.**

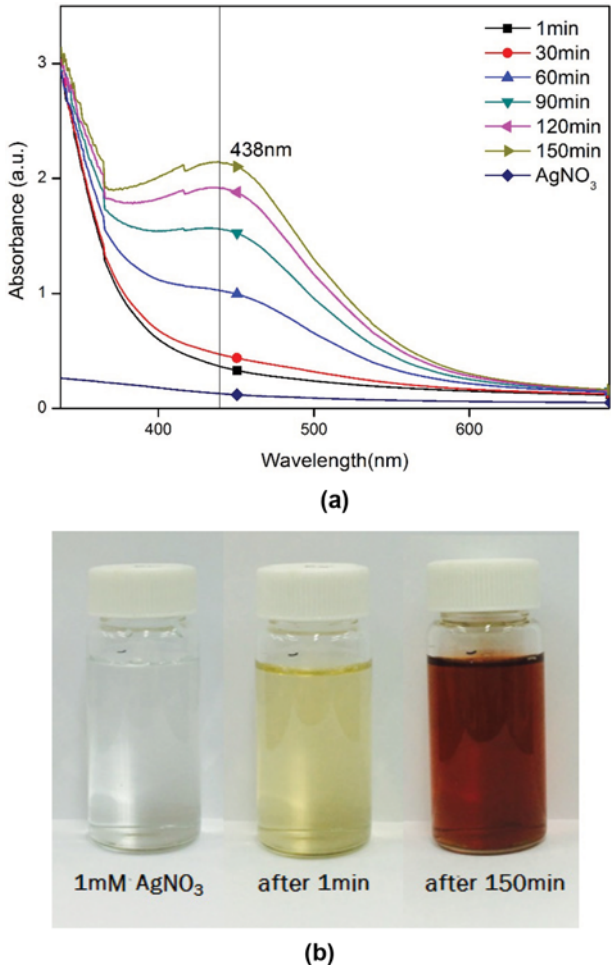


**Fig. 3. Time course of Ag nanoparticle synthesis by (a) UV-visible spectrophotometry and (b) color changes.**

monitored by different techniques. Fig. 1(a) shows the time course of CuO nanoparticle synthesis by UV-visible spectrum. The CuO aqueous dispersion shows an absorption peak at 368 nm. Fig. 1(b) shows the color changing from colorless of $CuSO_4 \cdot 5H_2O$ to dark brown of CuO nanoparticles. Likewise, the time courses of reduction of $KMnO_4$ to $MnO_2$ nanoparticles and $AgNO_3$ to Ag nanoparticles were monitored by UV-visible spectrum (Fig. 2(a) and 3(a)). The aqueous dispersion of $MnO_2$ and Ag showed an absorption peak at 404 and 438 nm, respectively. The colors changed from purple of $KMnO_4$ to dark brown for $MnO_2$ nanoparticles (Fig. 2(b)) and from colorless of $AgNO_3$ to red for Ag nanoparticles (Fig. 3(b)).

Fig. 4(a) shows XPS analysis of CuO nanoparticles. The binding energy of Cu2p for $Cu^{2+}$ is 934.3 eV ($Cu2p_{3/2}$) [30]. XPS analysis shows the existence of two binding energies for Cu2p for the CuO sample, 934.6 eV ($Cu2p_{3/2}$) and 954.5 eV ($Cu2p_{1/2}$), with a difference of 19.9 eV, proving the formation of copper(II) oxide. Hence, the satellite peak on the binding energy values higher than the main broad peak of $Cu^{2+}$ can be considered as a significant evidence of CuO composition presence [30]. Fig. 4(b) and Table 1 show EDS analysis and element composition of CuO nanoparticles. The Cu and O contents were found to be 4.1 atom% and 36.8 atom%. The result of EDS analysis shows high amount of carbon compound from plant leaf extracts. XPS, EDS, and element composition analysis of $MnO_2$ and Ag nanoparticles showed similar results with previously reported [14,15], proving the formation of $MnO_2$ and metallic Ag.

Fig. 5(a) to (c) show the SEM images of CuO, $MnO_2$, and Ag nanoparticles, indicating that relatively spherical nanoparticles are formed. The particle size and morphology of the nanoparticles was further determined using TEM. Observation of TEM image was prepared by dropping a few micro liters of dispersions onto the top holey carbon mesh grid. Fig. 6(a) to (c) show the TEM images of CuO, $MnO_2$, and Ag nanoparticles. The average particle size of CuO was 45.6 nm with diameter of particles ranging from 26 to 67 nm. The average particle sizes of $MnO_2$ and Ag were 19.2 nm (1-60 nm range) and 18.6 nm (5-35 nm range), respectively. All three nanoparticles were predominantly of spherical shape.

**2. Dye Degradation**

The three types of biosynthesized nanoparticles (CuO, $MnO_2$, and Ag) were examined to degrade Congo red and Safranin O. Dye degradation tests were performed by placing 0.01 g of the purified and freeze dried nanoparticles in contact with 1 mL of dye solution of 20 ppm for 10 min under constant stirring. Decolorization was monitored by UV-visible spectroscopy. Functional

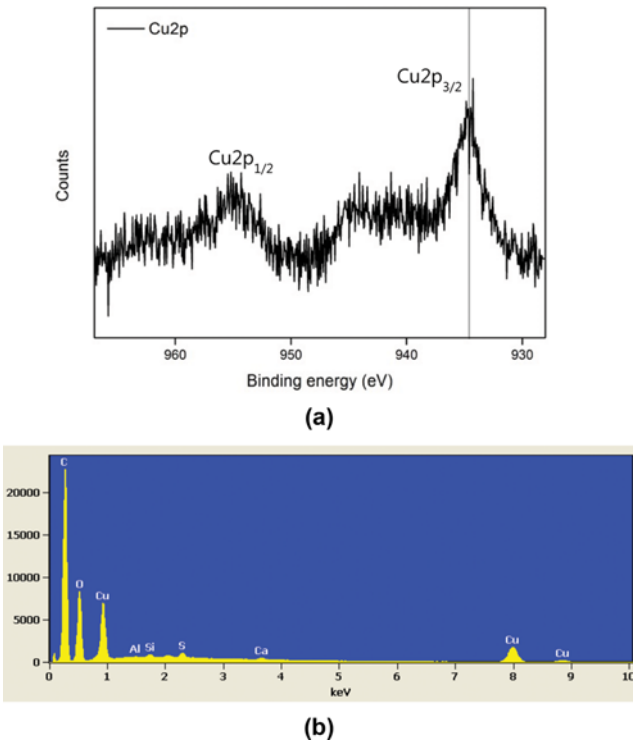


**Fig. 4. (a) XPS and (b) EDS analysis of CuO nanoparticles.**

groups before and after reactions were analyzed by FT-IR.

Fig. 7(a) shows time course of decolorization of Congo red by these nanoparticles. The ability of nanoparticles to remove dye was determined. Results showed that the decolorization by CuO nanoparticles increased to 57% after 1 min and then gradually decreased after 4 min. Almost 100% decolorization ability of Congo red was obtained with $MnO_2$ nanoparticles. The decolorization by Ag nanoparticles was about 65%. Fig. 7(b) shows spectra of Congo red before and after treatment with nanoparticles. Congo red shows absorption maximum at wavelength of 495 nm. Most peaks at 495 nm disappeared after treatment with $MnO_2$ nanoparticles and were considerably reduced after treatment with CuO and Ag nanoparticles. The difference in decolorization efficiency of nanoparticles may be due to differences in catalytic activity, shape, and size [15].

**Table 1. EDS analysis of elemental composition of CuO nanoparticles**

| Element | Weight% | Atom% |
|---|---|---|
| Cu | 16.45 | 4.07 |
| C | 44.57 | 58.36 |
| O | 37.41 | 36.77 |
| F | 0.17 | 0.1 |
| Mg | 0.51 | 0.29 |
| S | 0.58 | 0.29 |
| Ca | 0.31 | 0.12 |

Fig. 8(a) shows time course of decolorization of Safranin O by these nanoparticles. The decolorization ability to remove Safranin

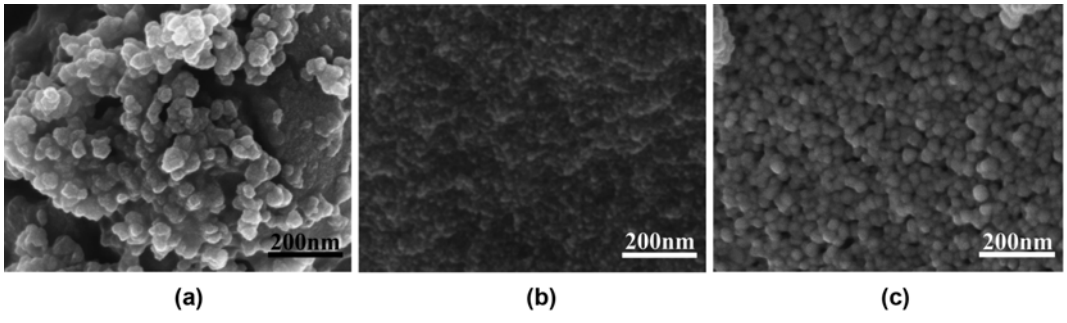


**Fig. 5. SEM image of (a) CuO, (b) $MnO_2$, and (c) Ag nanoparticles.**

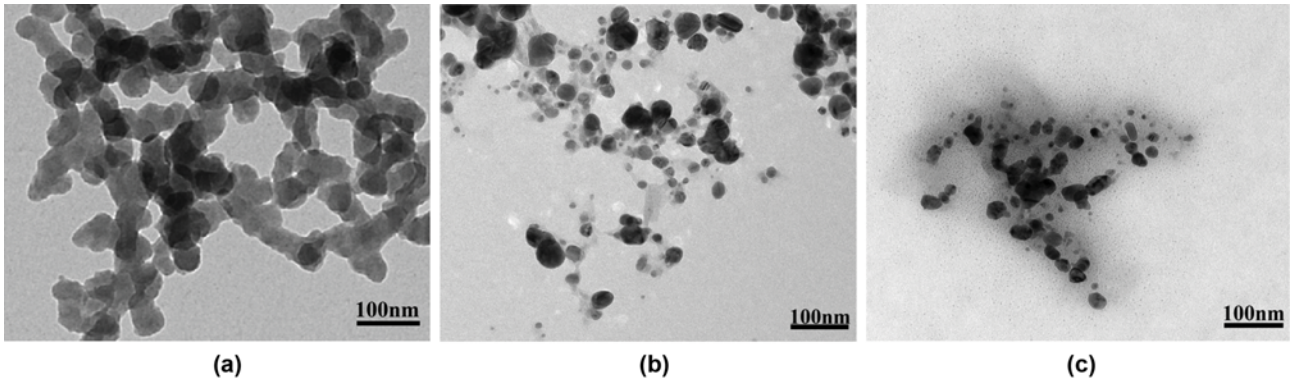


**Fig. 6. TEM image of (a) CuO, (b) $MnO_2$, and (c) Ag nanoparticles.**

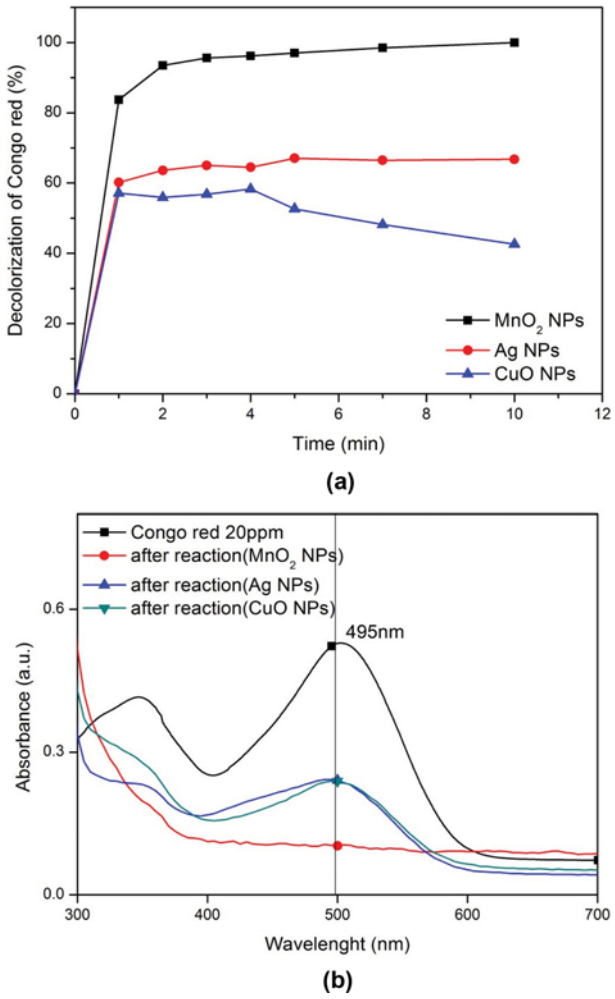


**Fig. 7. (a) Time course of decolorization of Congo red by nanoparticles and (b) spectra of Congo red before and after treatment with nanoparticles.**

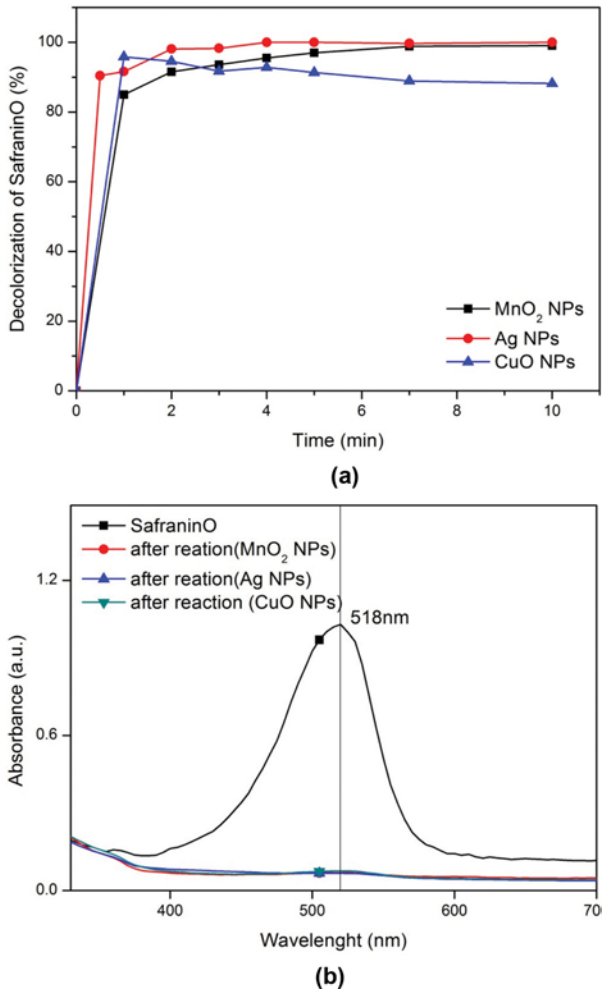


**Fig. 8. (a) Time course of decolorization of Safranin O by nanoparticles and (b) spectra of Safranin O before and after treatment with nanoparticles.**

O was similar at 90-100% for all nanoparticles. Fig. 8(b) shows spectra of Safranin O before and after treatment with nanoparticles. Safranin O shows absorption maximum at wavelength of 518 nm. After reaction, the peaks at 518 nm have almost disappeared after treatment with nanoparticles.

Fig. 9(a) shows the FT-IR analysis of Congo red before and after treatment with CuO nanoparticles. Fig. 9(b) shows chemical structure of Congo red. The FT-IR spectra of Congo red displays peaks at 3,467 $cm^{-1}$ for N-H stretching vibration of primary amine, 1,584 $cm^{-1}$ for aromatic -C=C- stretching vibration, 1,446 $cm^{-1}$ for -N=N- stretching vibration, 1,360 $cm^{-1}$ for -C-N bending vibration, and 1,062 $cm^{-1}$ for -S=O stretching vibration of sulfonic acid. The IR spectra after decolorization shows removed peak at 1,446 $cm^{-1}$ for -N=N- stretching vibration of chromophoric group in Congo red.

Fig. 10(a) shows the FT-IR analysis of Safranin O before and after treatment with CuO nanoparticles. Fig. 10(b) shows chemical structure of Safranin O. The FT-IR spectra of Safranin O displays peaks at 3,339 $cm^{-1}$ for-N-H stretching vibration of primary amine, 1,641 and 1,610 $cm^{-1}$ for aromatic ring stretching vibration, 1,493 $cm^{-1}$ for $-CH_3$ stretching vibration, and 1,334 $cm^{-1}$ for aromatic C=N stretching vibration. The IR spectra after decolorization show a removed peak at 1,334 $cm^{-1}$ for aromatic C=N stretching vibration of chromophoric group in Safranin O.

The catalytic dye degradation by Ag nanoparticles was explained by the electron transfer mechanism [26]. When a reducing agent such as $NaBH_4$ and a dye molecule are adsorbed on the large surface of the nanoparticles, the reduction potential of the nucleophilic $NaBH_4$ decreases and the reduction potential of the electrophilic dye molecule increases [26]. Electron transfer proceeds from a reducing agent to a dye molecule through metal nanoparticles, breaking the dye chromophore structure and forming a small species such as acetamide, $SO_4^{2-}$, $CO_2$, and $H_2O$ [26]. Because nanoparticles have a large surface area that serves as a substrate for electron transport reactions, nanoparticles act as efficient catalysts through electron transfer processes [31,32]. If there is a large potential difference between the electron donor and the acceptor, no electron transfer occurs. Nanoparticles can act as intermediate redox catalysts by promoting electron transfer [28,33]. Without a reducing agent such as $NaBH_4$, nanoparticles transfer electrons

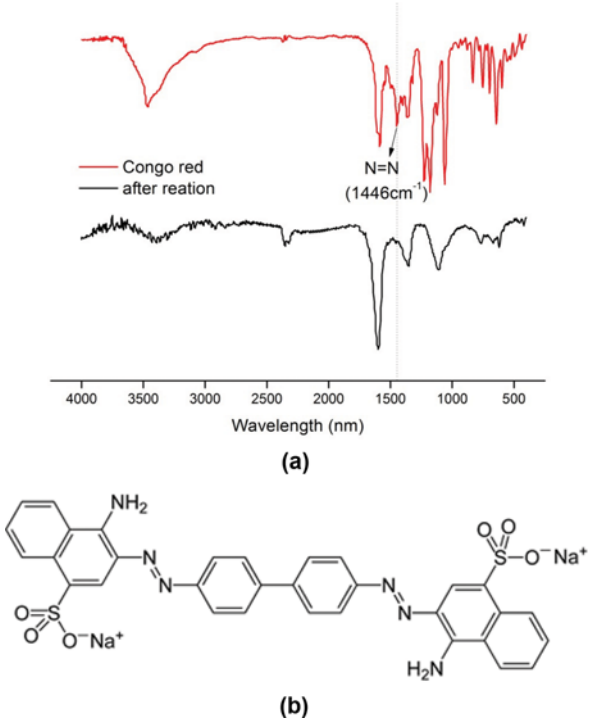


**Fig. 9. (a) FT-IR analysis of Congo red before and after treatment with nanoparticles and (b) chemical structure of Congo red.**

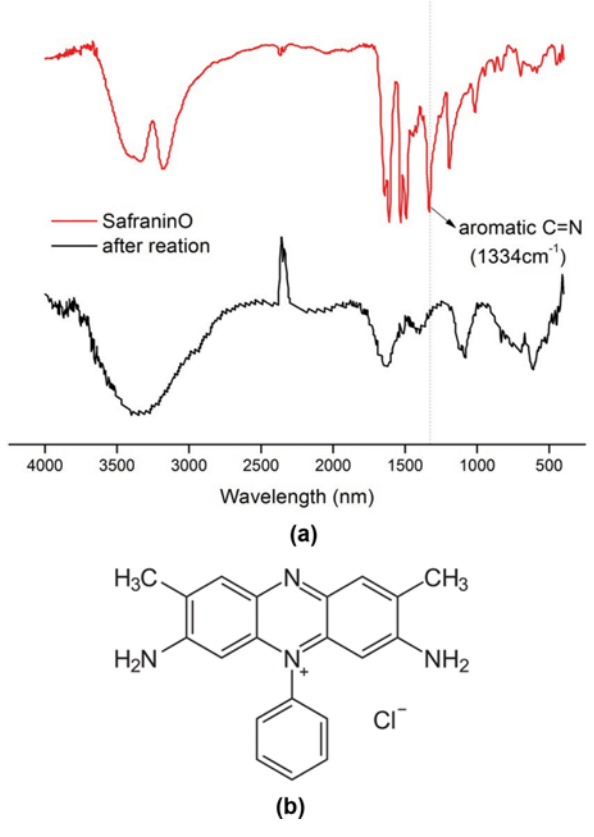


**Fig. 10. (a) FT-IR analysis of Safranin O before and after treatment with nanoparticles and (b) chemical structure of Safranin O.**

from plant metabolites to dyes, facilitating the reduction of dyes through electronic relay effects [15,28,34]. FT-IR studies also showed functional group change in dye molecules representing catalytic action of nanoparticles on dye molecules.

In summary, CuO, $MnO_2$, and Ag nanoparticles were synthesized using *Kalopanax pictus* plant extract. SEM and TEM analysis showed presence of the spherical nanoparticles with average size of 45.6, 19.2, and 18.6 nm for CuO, $MnO_2$, and Ag nanoparticles, respectively. The nanoparticles showed decolorization of Safranin O higher than 80%. The nanoparticle synthesis approach using plant extracts is possible with simple reactions that do not require catalyst, template or costly and precise equipment. This study will be useful for easy, cost-effective, reliable, and eco-friendly production of CuO, $MnO_2$, and Ag nanoparticles and their utilization for dye degradation.

## ACKNOWLEDGEMENTS

This research was supported by Small and Medium Business Administration (C0444488).

## REFERENCES

1. Willems, van den Wildenberg, Roadmap report on nanoparticles, W&W Espana sl, Barcelona, Spain (2005).
2. J. Y. Song and B. S. Kim, *Bioproc. Biosyst. Eng.*, **32**, 79 (2009).
3. B. K. Salunke, E. Sathiyamoorthi, T. K. Tran and B. S. Kim, *Korean J. Chem. Eng.*, **34**, 943 (2017).
4. H. Bar, D. K. Bhui, G. P. Sahoo, P. Sarkar, S. P. De and A. Misra, *Colloid Surf. A*, **339**, 134 (2009).
5. P. Dauthal and M. Mukhopadhyay, *Korean J. Chem. Eng.*, **32**, 837 (2015).
6. B. K. Salunke, S. S. Sawant, S. I. Lee and B. S. Kim, *Appl. Microbiol. Biotechnol.*, **99**, 5419 (2015).
7. B. K. Salunke, S. S. Sawant, S. I. Lee and B. S. Kim, *World J. Microb. Biot.*, **32**, 1 (2016).
8. N. Saifuddin, C. W. Wong and A. A. Yasumira, *E-J. Chem.*, **6**, 61 (2009).
9. G. M. Gadd, O. S. Laurence, P. A. Briscoe and J. T. Trevors, *Biol. Met.*, **2**, 168 (1989).
10. I. Willner, R. Baron and B. Willner, *Adv. Mater.*, **18**, 1109 (2006).
11. M. Zayats, R. Baron, I. Popov and I. Willner, *Nano Lett.*, **5**, 21 (2005).
12. B. K. Salunke, S. V. Patil, R. Lad, S. Chatterjee and V. L. Maheshwari, *J. Cell Tissue Res.*, **8**, 1545 (2008).
13. H. P. Borase, B. K. Salunke, R. B. Salunkhe, C. D. Patil, J. E. Hallsworth, B. S. Kim and S. V. Patil, *Appl. Biochem. Biotechnol.*, **173**, 1 (2014).
14. B. K. Salunke, J. Shin, S. S. Sawant, B. Alkotaini, S. Lee and B. S. Kim, *Korean J. Chem. Eng.*, **31**, 2035 (2014).
15. S. A. Moon, B. K. Salunke, B. Alkotaini, E. Sathiyamoorthi and B. S. Kim, *IET Nanobiotechnol.*, **9**, 220 (2015).
16. H. Wang, J. Z. Xu, J. J. Zhu and H. Y. Chen, *J. Cryst. Growth*, **244**, 88 (2002).
17. A. El-Trass, H. ElShamy, I. El-Mehasseb and M. El-Kemary, *Appl. Surf. Sci.*, **258**, 2997 (2012).

18. K. Zhang, Y. Yang, E. Y. B. Pun and R. Shen, *Nanotechnology*, **21**, 235602 (2010).
19. X. Y. Chen, H. Cui, P. Liu and G. W. Yang, *Appl. Phys. Lett.*, **90**, 183118 (2007).
20. T. Kimura, Y. Sekio, H. Nakamura, T. Siegrist and A. P. Ramirez, *Nat. Mater.*, **7**, 291 (2008).
21. M. K. Sahu, U. K. Sahu and R. K. Patel, *RSC Adv.*, **5**, 42294 (2015).
22. N. M. Mahmoodi, M. Arami, N. Y. Limaee and N. S. Tabrizi, *Chem. Eng. J.*, **112**, 191 (2005).
23. I. K. Konstantinou and T. A. Albanis, *Appl. Catal. B-Environ.*, **49**, 1 (2004).
24. K. K. Dehury, MSc Thesis, National Institute of Technology, Rourkela, Odisha, India (2014).
25. N. Dizge, C. Aydiner, E. Demirbas, M. Kobya and S. Kara, *J. Hazard. Mater.*, **150**, 737 (2008).
26. G. M. Patel, *Nanomaterials: preparation, characterisation and application*, Ph.D. Thesis, Gujarat University, India (2009).
27. H. P. Borase, C. D. Patil, R. B. Salunkhe, R. K. Suryawanshi, B. K. Salunke and S. V. Patil, *Bioproc. Biosyst. Eng.*, **37**, 1695 (2014).
28. K. Roya, C. K. Sarkar and C. K. Ghosh, *Dig. J. Nanomater. Bios.*, **10**, 107 (2015).
29. M. L. Chacón-Patiño, C. Blanco-Tirado, J. P. Hinestroza and M. Y. Combariza, *Green Chem.*, **15**, 2920 (2013).
30. O. Akhavan and E. Ghaderi, *Surf. Coat. Tech.*, **205**, 219 (2010).
31. S. K. Ghosh, S. Kundu, M. Mandal and T. Pal, *Langmuir*, **18**, 8756 (2002).
32. V. K. Vidhu and D. Philip, *Micron*, **56**, 54 (2014).
33. R. M. Tripathi, N. Kumar, A. Shrivastav, P. Singh and B. R. Shrivastav, *J. Mol. Catal. B-Enzym.*, **96**, 75 (2013).
34. K. Mallick, M. Witcomb and M. Scurrell, *Mater. Chem. Phys.*, **97**, 283 (2006).